Data Processing at the Flaw Detector with Combined Multisector Eddy-Current Transducer

Evgeny Yakimov, Alexander Goldshtein, Valery Bulgakov, Sergey Shipilov
National Research Tomsk Polytechnic University- Institute of Nondestructive Testing
Lenina Ave. 30, Tomsk, 634050, Russia
E-mail: shishkovka@mail.ru, algo154@yandex.ru, bvf49@sibmail.com, shipilov@webmail.tsu.ru

***Abstract*—There is described data processing at the flaw detector with combined multisectional eddy-current transducer and heterofrequency magnetic field. The application of this method for detecting flaws in rods and pipes under the conditions of significant transverse displacements is described.**

***Keywords*: combined multisector eddy-current transducer, eddy-current testing, nondestructive testing of bars and tubes.**

I. Introduction

At flaw detecting of extended metal articles (rods and pipes) in a process of production there are problems caused by heavy testing conditions. Firstly, it is necessary to provide independence from the large transverse displacements of controlled product. Secondly, it is necessary to detect defects with different physical natures and geometrical parameters: faulty fusions, cracks, hair cracks, rolling laps, nonmetallic inclusions. Thirdly, electromagnetic properties of controlled article material could vary from sample to sample. It makes difficult calibration of the flaw detector. Cause of the difference in electromagnetic properties could be variation of temperature and different chemical composition of material.

Above mentioned problems could be solved using combination attachable multisector ECT (eddy-current transducer) and transmission multisector ECT with excitation of circularly and longitudinally directed ECs (eddy-currents) at different frequencies [1][2]. Advantages of such technical solution are high sensitivity to both local defects and extended defects in the presence of large transverse displacements between surface of tested object and windings of ECT, small dependence of signal from the position of defect in the control zone and transverse displacement of the object.

Effective detuning from the influence of transverse displacements can be provided even by the large change of electromagnetic properties [3].

II. Flaw Detector with Transmission Multisector and Attachable Multisector Eddy-Current Transducer

Fig. 1a shows the structural scheme of the FD (flaw detector) in which the proposed testing method is implemented and Fig. 1b shows the design of the ECT of the FD. For clearness, the ECT windings are conditionally separated along the longitudinal Z axis, but in reality, all the winding have the same longitudinal location.

The FD principle of operation is as follows. Generators *1–3* generate harmonic voltages at frequencies ω_1, ω_2, and ω_3. All generators are synchronized by synchronization circuit *4*; due to this, the frequency differences $\omega_2-\omega_1=\Delta\omega$ and $\omega_3-\omega_1=k\Delta\omega$ (here, k is an integer) are maintained at stable levels. The frequencies ω_1, ω_2, and ω_3 differ from $\Delta\omega$ by an integer number of times. In this case, different variants of synchronizing the generator frequencies are possible, for example, a variant where the synchronization circuit contains a generator of rectangular pulses of the reference frequency ω_0, and generators *1–3* contain frequency dividers by factors of $m(n-1)$, mn, and $n(n-1)$, respectively, and the selective circuits for selecting the first harmonics of rectangular signals (m and n are integers). In this case, the frequencies of the output voltages of the generators are, respectively, $\omega_1=\omega_0/mn$, $\omega_2=\omega_0/m(n-1)$, and $\omega_3=\omega_0/n(n-1)$.

The frequency difference is $\Delta\omega=\omega_0/mn(n-1)$ and $k=m-n+1$. The signal of the difference frequency $\Delta\omega$ can be obtained by the consecutive division of the frequency ω_0 by m, n, and $(n-1)$. This signal is used for processing ECT signals.

The output signals of generators *1–3* are fed to the excitation windings *5–7* of the ECT. The currents in these windings create a magnetic field with three harmonic orthogonal spatial frequency components ω_1, ω_2, and ω_3 in the ECT testing zone. The three frequencies exciting magnetic field induces eddy currents at three frequencies in a tested article. The two-sectional attachable-type windings *5* and *6* are used to excite longitudinal eddy currents at frequencies ω_1 and ω_2, which have close values, in the surface layer of a tested article. Transmission-type winding *7* serves for exciting eddy currents of circular direction at the frequency ω_3. Note that, in this case, in contrast to the use of classical multifrequency ECTs, the frequency difference $\Delta\omega$ is negligibly small from the standpoint of the results of electrodynamic interaction of the magnetic field with a tested object.

In order to reduce signals from structural inhomogeneities that usually correlate with local changes in the magnetic properties, magnetic biasing of a tested object is performed in the FD by the magnetic field of a direct current in magnetization winding *17*, which is connected to stabilized magnetizing-current source *16*.

To measure the components of the field of eddy currents at the frequencies ω_1 and ω_2, four-sectional and two-sectional measuring windings *8* and *9* and two-sectional and four-sectional measuring windings *10* and *11* are used, respectively. The components of the field of eddy currents at the frequency ω_3 are measured with one-sectional measuring windings *12–15*. Owing to the appropriate directions of coiling the sections of the exciting and measuring windings and their mutual arrangement (Fig. 1b), when an article is absent in the ECT testing zone and the axis of an article, which is placed in the testing zone, coincides with the longitudinal axis of the ECT, the initial and introduced EMF (electromotive force) of the measuring windings at the frequency of the measured magnetic field are absent. This property of the ECT that is used in the FD makes the latter poorly sensitive to such interfering factors as changes in the diameter and the electromagnetic properties within the acceptable range for a suitable article. An EMF at the frequency of the measured magnetic field in the measuring windings arises upon disturbance of the symmetry of eddy currents that are induced in an article in the presence of a flaw, a radial displacement (for windings *8–11*), or a skew (for windings *8–15*) of a tested article relative to the longitudinal axis of ECT.

Amplitude–phase processing of signals is used to separate these effects. For this purpose, the FD has ten identical measuring channels *18–25*, each of which consists of an amplitude–phase detector and an integrating digitizer that connected in series. Channels *18–21* are intended for selecting signals from extended flaws, channels *18* and *20* are intended, in addition, for selecting signals from transverse displacements of a tested article along the *Y* and *X* axes, respectively, and channels *22–25* are intended for selecting signals from short flaws.

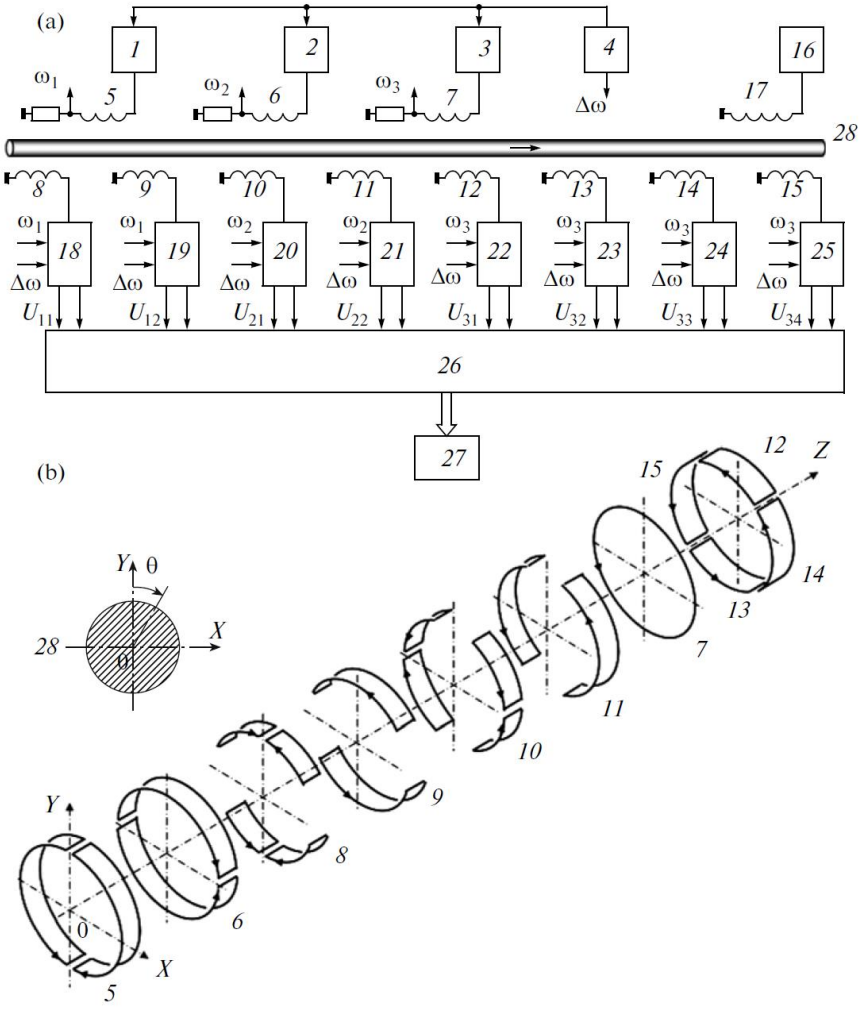

Fig. 1. (a) Structural diagram and (b) the design of the ECT of a flaw detector: (*1–3*) generators, (*4*) synchronization scheme, (*5–7*) excitation windings, (*8–15*) measuring windings, (*16*) magnetizing current unit, (*17*) magnetizing winding, (*18–25*) measuring channels, (*26*) calculation unit, (*27*) actuating devices, and (*28*) tested object

The amplitude–phase detector performs synchronous detection of the voltage across the measuring ECT winding with the corresponding control frequency ω_i and the integrating digitizer averages the output signal of the amplitude–phase detector over the time $T = 2\pi / \Delta\omega$, which is set by the output signal of synchronization circuit *4*. The integrating digitizer circuit includes the circuits of an analog integrator and a storage unit, which are connected in series and over which a negative feedback loop is placed, and is a pulsed low-pass filter with a finite pulsed characteristic [4]. The transfer coefficient of such measuring channel has the following dependence on the input signal frequency ω:

$$K(\omega) = \frac{T}{2} \int_{-T/2}^{T/2} \sin \omega t \cdot \sin \omega_i t \cdot \mathrm{d}t = \frac{2}{\pi} \cdot \frac{\omega_i \cdot \Delta\omega}{\omega^2 - \omega_i^2} \cdot \sin \pi \frac{\omega}{\Delta\omega} \qquad (1)$$

The analysis of the amplitude–frequency characteristic (AFC) of the measuring channel (Fig. 2) with a reference frequency ω_i (curve *1*) shows that the dependence $K(\omega)$ has zeros at frequencies that differ from ω_i by values multiple of $\Delta\omega$. A modulated signal at a frequency ω_i from a flaw with the spectrum shown in Fig. 2 is transmitted by the measuring channel almost without distortions and a modulated signal at a nearby frequency $\omega_i+\Delta\omega$ (its spectrum is shown by curve *3*) is attenuated by more than one order of magnitude. It is also important that slowly changing signals at the frequency $\omega_i+\Delta\omega$ (drift of the unbalance voltage, displacement-caused signals) are completely suppressed by the measuring channel even when the values of ω_i and $\omega_i+\Delta\omega$ are very close to each other.

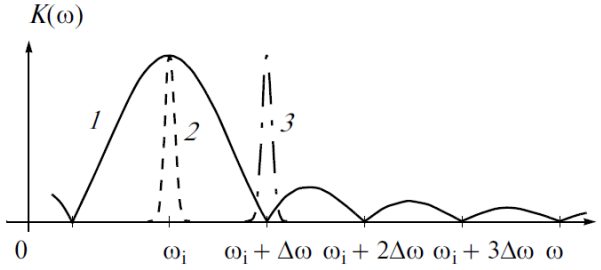

Fig. 2. The amplitude–frequency characteristic of the measuring channel with a reference frequency ω_i.

As a result of such signal processing, signals U_{11} and U_{12} are extracted at the outputs of measuring channels *18* and *19*. These signals are proportional to the amplitudes of the complex components of the introduced voltages of four-sectional and two-sectional measuring windings *8* and *9*, respectively, at the frequency ω_1. Signals U_{21} and U_{22} are extracted at the outputs of measuring channels *20* and *21*. These signals are proportional to the amplitudes of the complex components of the introduced voltages of four_ and

Two-sectional measuring windings *10* and *11*, respectively, at the frequency ω_2. Signals U_{31}, U_{32}, U_{33}, and U_{34}, which are proportional to the amplitudes of the complex components of the introduced voltages of one-sectional measuring windings *12–15* at the frequency ω_3, are extracted at the outputs of measuring channels *22–25*.

The high quality separation of signals that are caused by each separate magnetic field component allows efficient use of the amplitude–phase tuning out from the influence of radial displacements and skews. This kind of tuning out in each channel is performed by regulating the phase shifts of the reference voltages of the amplitude–phase detectors. The voltages across resistors, which are connected in series with the excitation windings, which coincide in phase with the ECT excitation currents, are used as the reference voltages in the FD circuit. For the measuring channels with the frequencies ω_1 and ω_2, the direction of the tuning out from displacements, which is orthogonal to the displacement line, virtually coincides with the line of flaws for the used ECTs and testing conditions; for the measuring channels with the frequency ω_3, the direction of the tuning out makes an angle of 30–45° with the lines of flaws. As a result of the amplitude–phase tuning out, the imaginary components of the output voltages of the FD's measuring channels are determined mainly by the presence or absence of a defective zone of the article in the tested zone and the real components are determined by the transverse displacement of the article relative to the longitudinal axis of the ECT.

Calculation unit *26* determines the resulting voltages U_1 of the measuring channels of the longitudinal components of eddy currents at the frequencies ω_1 and ω_2 and U_2 of the measuring channels of the circular components of eddy currents at the frequency ω_3. In addition, unit *26* compares these voltages to specified threshold values.

The signal amplitudes from a flaw in each measuring channel depend not only on the flaw geometry (depth, opening, and orientation), but also on the azimuth (angle θ of the location on the article surface (Fig. 1b).

Fig. 3 shows the dependences of the flaw-introduced voltages of the channels for extracting signals from extended flaws on the flaw azimuth. For the amplitude of the total signal to be independent of the azimuth of an extended flaw, the pairwise algebraic summation is performed and signals from flaws of measuring channels *18–21* are then vector summed:

$$U_1 = \sqrt{(\mathrm{Im}\dot{U}_{11} + \mathrm{Im}\dot{U}_{22})^2 + (\mathrm{Im}\dot{U}_{12} + \mathrm{Im}\dot{U}_{21})^2} \qquad (2)$$

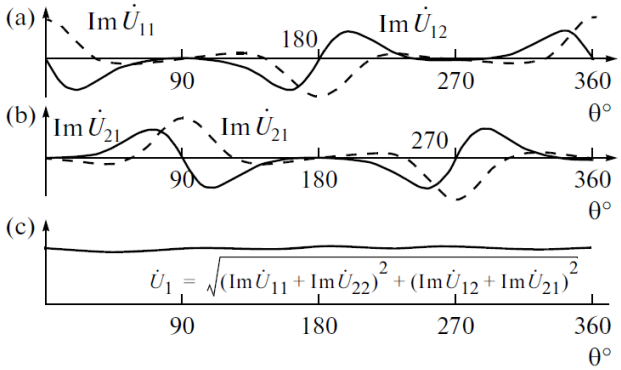

Fig. 3. The dependences (a, b) of the flaw-introduced voltages of individual FD channels and (c) the resulting signal on the flaw azimuth.

The resulting signal U_1 is virtually independent of the flaw azimuth. Another positive feature of this algorithm for processing ECT signals is that, in this case, a noise signal that is caused by the possible violation of the optimal condition of tuning out from a displacement because of changes in the electrophysical properties of a tested article

and a disturbance of the perpendicularity of the tuning out direction and the displacement line, is substantially attenuated. Physically, this weakening of the influence of the displacement is explained by the fact that when the article shifts along the *OY* and *OX* axes signals arise in measuring windings *8–11* and *9–10*, respectively; these signals are in antiphase in both cases. As a result, after the detected voltages are summed, signals from the displacement in different channels are mutually compensated.

For the amplitude of the total signal U_2 to be independent of the azimuth of a short flaw and in order to weaken the dependence of U_2 on transverse displacements of a tested article, the output signals from flaws of measuring channels *22–25* are algebraically summed in calculation unit *26* by analogy with [5] with coefficients s_1, s_2, s_3, and s_4, respectively, which are calculated as functions of the values of transverse displacement of the article.

The necessity of using correcting coefficients during summation of signals from short flaws is determined by the much stronger dependence on the transverse displacements of a tested article than in the case of extended flaws.

Fig. 4 shows the behavior of the dependences of the output signals from a flaw of measuring channels *22–25* $\mathrm{Im}U_{31}$, $\mathrm{Im}U_{32}$, $\mathrm{Im}U_{33}$, and $\mathrm{Im}U_{34}$ on the flaw azimuth θ for a transverse displacement of a tested article along the *OY* axis (y=–2mm). All the dependences are normalized to the maximum signal from the flaw in the measurement channels without a displacement.

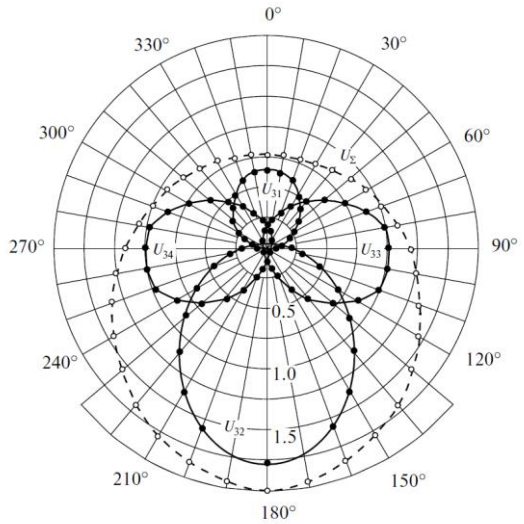

Fig. 4. Dependences of signals of the measuring channels on the flaw azimuth during a transverse displacement of a tested article by 2 mm to winding *14*.

The analysis of the curves in Fig. 4 shows that the flaw-introduced signals in measuring channels *23* and *25*, which are connected to windings *13* and *15*, are virtually independent of a transverse displacement of the mentioned direction. During a transverse displacement in the given direction, the flaw-introduced signal in measuring channel *22*, which is connected to winding *12*, decreases by a factor of 1.54; the flaw-introduced signal in measuring channel *24*, which is connected to winding *14*, increases by a factor of 1.76.

A dotted line shows the total signal U_Σ of all four measuring channels without using correcting coefficients.

In this case, the degree of nonuniformity of the sensitivity to a flaw, which is caused by transverse displacements, reaches 160%.

The initial data for determining the correcting coefficients $s1$, $s2$, $s3$, and $s4$ are the dependences of signals from flaws of measuring channels *22–25* $\mathrm{Im}U_{31}$, $\mathrm{Im}U_{32}$, $\mathrm{Im}U_{33}$, and $\mathrm{Im}U_{34}$ and signals from displacements of measuring channels *18* and *20* $\mathrm{Re}U_{11}$ and $\mathrm{Re}U_{21}$on transverse displacements x and y along the *OX* and *OY* axes, respectively.

Fig. 5 shows the behavior of the dependences of the signals $\mathrm{Im}U_{31}(y)$ and $\mathrm{Im}U_{32}(y)$ from flaws on a transverse displacement y along the *OY* axis and the signal $\mathrm{Re}U_{11}(y)$ on the displacement. These dependences can be represented by the following functions:

$$\mathrm{Im}U_{31}(y) = F_1(y)U_{N1};\ \mathrm{Im}U_{32}(y) = F_2(y)U_{N2};\ \mathrm{Re}U_{11}(y) = F_3(y) \tag{3}$$

Here, U_{N1} and U_{N2} are signals from a flaw in the absence of a displacement (y=0), $F_1(y)$ and $F_2(y)$ are functions that describe the dependences of signals from the flaw on the displacement, and $F_3(y)$ is a function that describes the dependences of a displacement-caused signal on the displacement.

The function $F_3(y)$ can be considered linear with a sufficient degree of accuracy:

$$\mathrm{Re}U_{11}(y) = t\,y \tag{4}$$

where

t - a constant factor.

From here, the displacement value can be determined:

$$y = \frac{\mathrm{Re}U_{11}}{t} \tag{5}$$

Using the calculated value of y, the displacement independent values of signals from a flaw can be determined:

$$U_{N1} = \frac{\mathrm{Im}U_{31}}{F_1(y)} \text{ and } U_{N2} = \frac{\mathrm{Im}U_{32}}{F_2(y)} \tag{6}$$

Thus, the correcting coefficients are

$$s_1 = \frac{1}{F_1(y)} \text{ and } s_2 = \frac{1}{F_2(y)} \tag{7}$$

In view of the same character of the dependences of signals on displacements x and y, the displacements x and the correcting coefficients are found in a similar manner:

$$s_3 = \frac{1}{F_1(x)} \text{ and } s_4 = \frac{1}{F_2(x)} \tag{8}$$

The functional dependences $F_1(y)$ and $F_2(y)$ and the value of the factor t are usually determined experimentally. The functions $F_1(y)$ and $F_2(y)$ are specified in calculation unit *26*

in a tabulated form or are approximated by analytical expressions. The resulting signal U_2 of channels for measuring the circular components of eddy currents at the frequency ω_3 is equal to

$$U_2 = s_1 \operatorname{Im} U_{31} + s_2 \operatorname{Im} U_{32} + s_3 \operatorname{Im} U_{33} + s_4 \operatorname{Im} U_{34} \quad (9)$$

and is virtually independent of the flaw azimuth; it depends weakly on the transverse displacement of a tested article. The degree of nonuniformity of the sensitivity of a flaw, which is caused by transverse displacements, decreases owing to the above described transformation to an acceptable value of ~20%.

When the voltages U_1 and U_2 exceed the threshold values, the calculation unit forms a control signal for actuating devices *27* (rejection-bin control relay, paint marker, etc.).

III. Conclusion

The proposed flaw detection method was implemented in a FD prototype. Tests confirmed that such method has high sensitivity to both local defects and extended defects in the presence of large transverse displacements of tested object, small dependence of signal from the position of defect in the control zone and transverse displacement of the object.

References

[1] A. E. Goldshtein, V. F. Bulgakov, and H._M. V. A. Kroning, “A Method of Eddy-Current Flaw Detection of Bars and Tubes Based on the Use of a Combined Eddy-Current Transducer with Excitation of Spatial Magnetic-Field Components at Different Frequencies,” Russian Journal of Nondestructive Testing, Vol. 47, No. 11, pp. 747-753, 2011.

[2] A. A. Polevoda and I. Yu. Fedosenko, “On Eddy-Current Flaw Detection with Transmission Transducers for Flow-Line Testing of Pipes and Rolled Stocked, Zavod. Lab., Vol. 64, No. 1, pp. 34–37, 1998.

[3] V. K. Zhukov and P. A. Ovsyannikov, “ED-3.02 Electromagnetic Flaw Detector for Testing Long Cylindrical Articles,” Defektoskopiya, No. 4, pp. 30–36, 1983.

[4] A. E. Goldshtein and S. A. Kalganov, “Eddy-Current Nondestructive Testing of Long Cylindrical Articles Using Spatial Magnetic-Field Components of Different Frequencies”, Defektoskopiya, No. 5, pp. 65–71, 2000.

[5] V. F. Bulgakov, “Decrease in the Nonuniformity of the Sensitivity of Eddy-Current Transducers under Radial Displacements of Tested Articles”, Defektoskopiya, No. 9, pp. 3–8, 1999.